Investigating Intrinsic Attenuation in Large Low Velocity Provinces

COLLEGE OF COMPUTER, MATHEMATICAL, & NATURAL SCIENCES
DEPARTMENT OF GEOLOGY

MARYLAND SEISMOLOGY

Donovan Cunion | Advisor: Dr. Ved Lekic | GEOL394
Department of Geology, University of Maryland at College Park

Introduction

LLVPs are massive anomalous regions at the core-mantle-boundary that have raised questions about the evolution of Earth's mantle. These regions are seismically slow for S and P waves, commonly explained by thermochemical heterogeneity (Fig. 1). Constraints on the material properties of these regions will allow for a better understanding of their possible origins and present- day role in mantle dynamics. Constraints on temperature and composition based on velocity alone are non-unique, therefore this study aims to provide collaborating evidence through stronger constraints on seismic attenuation.

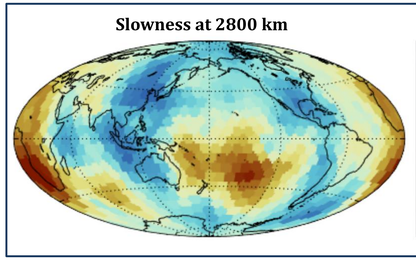

Fig. 1: Tomographic model of velocity inverted from S, SS, SSS, and ScS travel times. Higher slowness is plotted in warm colors. The warmest regions show the separate Pacific and African LLVP regions.

Attenuation Background

$$Q = Q_0 \exp\left(\frac{\alpha H^*}{RT}\right)$$

Eq 1. The inverse of attenuation (Q) has an exponential relationship with temperature(T), enthalpy (H*), and the frequency-dependence of attenuation (α) and a linear relationship with Q_0. Q_0 is primarily a factor of grain size in the lower mantle

High attenuation relates to hotter temperature and/or smaller grain size
Low attenuation relates to colder temperature and/or larger grain size

The two published models of lower mantle attenuation resolve opposite Q perturbations for LLVP regions (Fig. 2). The more recent QL3S4 (Talavera-Soza et al. 2025) depicts low relative attenuation in LLVPs. This contrasts with previous thermally-dominated anelasticity in LLVPs predicted by QLM9 (Lawrence and Wysession, 2006).

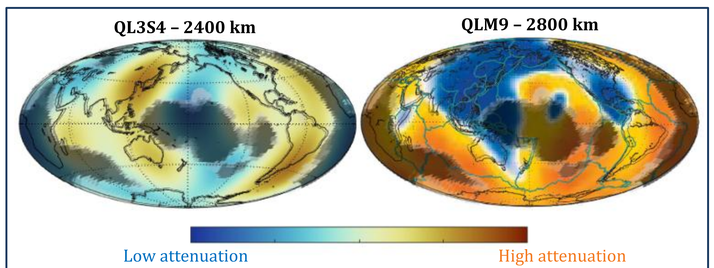

Fig. 2: Global attenuation of the lower mantle with LLVPs shown as shaded regions.

Hypotheses

NULL: Time spent in LLVPs has no effect on attenuation of body waves (t*)

HY1: QLM9 agreement; LLVPs are more attenuating than the ambient lower mantle

HY2: QL3S4 agreement; LLVPs are less attenuating than the ambient lower mantle

Methods

The data in this study are the t* measurements from Lai and Garnero (2019; 2020). t* is the total attenuation accumulated over a wave path, expressed as anelastic delay time (s). Analysis of the lower mantle requires correcting for the attenuation signal accumulated in the upper mantle. This study uses two independent methods to focus on lower mantle signal: ScS-S differential t* and path correction based on published upper mantle Q models.

ScS-S δt*

$$t^* = \int_{path} \frac{1}{Q(\vec{x})}\, dt$$

Eq 2. Anelastic delay time is an integration of the time a wave spends in a region with a certain Q.

ScS and S wave with similar source and receiver locations will take similar paths in the upper mantle. These waves spend travel the same path for a portion of the upper mantle, therefore the difference between their t* shows the attenuation differences between the mid and lower mantle. ScS and S wave are filtered by epicentral distances between 50 and 80 degrees to ensure path similarity and sensitivity to lowermost mantle.

Path Correction

$$t^* = \sum_j \frac{1}{Q_j} \Delta t_j$$

Eq 3. t* can be discretized to represent a summation over non-continuous regions with an assigned Q in each given region.

The path each wave takes is predicted using TauP toolkit (Crotwell et al., 1999) for the PREM model. This path is used to predict t* for upper mantle Q models QRSFI12 and SEMUCBQ (Dalton et al., 2008; Karaoglu & Romanowicz, 2018). Values outside the model space are set to an average lower mantle Q (558). The predicted t* for each model is subtracted from the observed t* to find the deviations from average in the lower mantle.

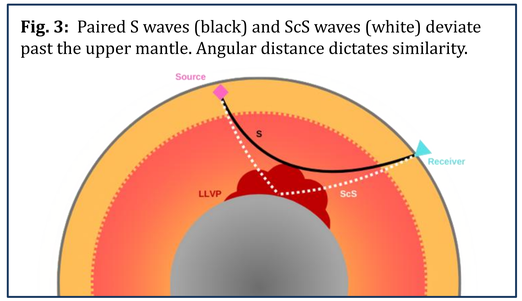

Fig. 3: Paired S waves (black) and ScS waves (white) deviate past the upper mantle. Angular distance dictates similarity.

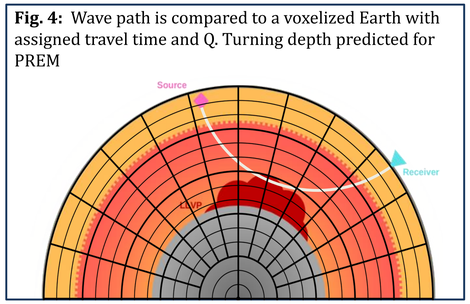

Fig. 4: Wave path is compared to a voxelized Earth with assigned travel time and Q. Turning depth predicted for PREM

Coverage

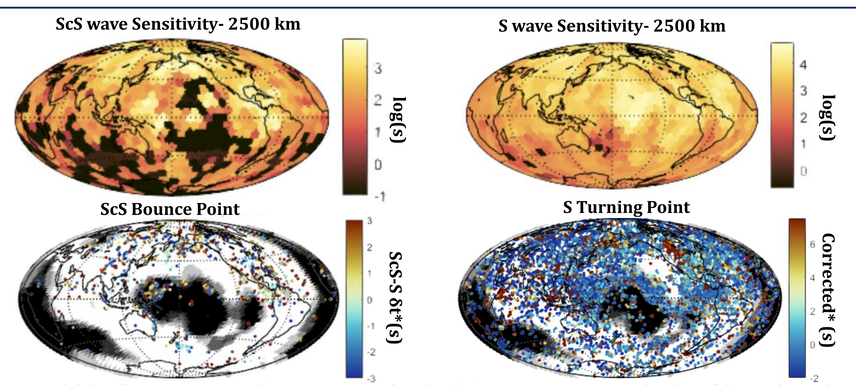

Fig. 5: Data availability for ScS-S pairs and S waves at 2500 km depth. Sensitivity is expressed as log of the total travel time in the regions. Below is the bounce and turning points for waves compared to LLVP vote maps.

Results: Differential ScS-S t*

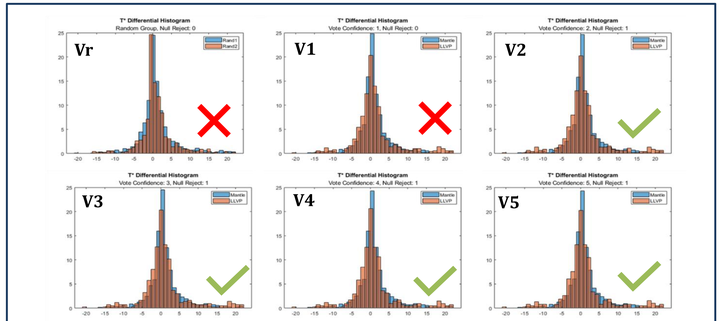

Fig. 6: t* distributions for ScS wave bounce points compared to LLVP votemap from Cottaar and Lekic (2016). Vr and V1 show identical distribution under the Mann-Whitney U test. V2-V5 reject the null hypothesis.

Results: Path Correction

The difference in observed and predicted t* increases with time spent in LLVPs (defined at V3). This high attenuating relationship is interpreted as a high temperature, low viscosity LLVP material. Results are more consistent with QLM9 than QRFSI12 , rejecting hypothesis 2.

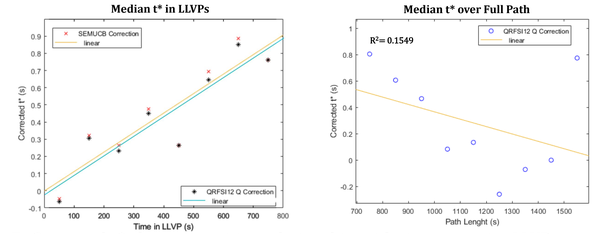

Fig. 7: Corrected t* shows a positive relationship with time spent in LLVPs not observed in total path time (SEMUCB R^2 = 0.7968; QRFSI R^2 = 0.8227). LLVPs must have a lower Q than the calculated average for the lower mantle to produce this relationship.

Conclusions

LLVPs have higher attenuation
- Approximations (self-coupling) adversely affect anelastic models (QL3S4)
- Thermally dominated anelasticity → low viscosity LLVPs

LLVPs have higher attenuation only at body wave frequencies
- Frequency dependance of attenuation is important in lower mantle
- Absorption band for LLVP material could vary from the surrounding material

References

Cottaar, S., & Lekic, V. (2016). Morphology of seismically slow lower-mantle structures. Geophysical Journal International, 207(2), 1122–1136.
Crotwell, H. P., Owens, T. J., & Ritsema, J. (1999). The TauP Toolkit: Flexible Seismic Travel time and Ray-path Utilities. Seismological Research Letters, 70(2), 154–160.
Dalton, C. A., Ekström, G., & Dziewoński, A. M. (2008). The global attenuation structure of the upper mantle. Journal of Geophysics
Dziewoński, A. M., & Anderson, D. L. (1981). Preliminary reference Earth model. Physics of the Earth and Planetary Interiors, 25(4), 297–356cal Research: Solid Earth, 113(B9).
Karaoğlu, H., & Romanowicz, B. (2018). Inferring global upper-mantle shear attenuation structure by waveform tomography using the spectral element method. Geophysical Journal International, 213(3), 1536–1558.
Lai, H., & Garnero, E. J. (2020). Travel Time and Waveform Measurements of Global Multibounce Seismic Waves Using Virtual Station Seismogram Stacks. Geochemistry, Geophysics, Geosystems, 21(1),
Lai, H., Garnero, E. J., Grand, S. P., Porritt, R. W., & Becker, T. W. (2019). Global Travel Time Data Set From Adaptive Empirical Wavelet Construction. Geochemistry, Geophysics, Geosystems, 20(5), 2175–2198.
Lawrence, J. F., & Wysession, M. E. (2006). Seismic Evidence for Subduction-Transported Water in the Lower Mantle. In Earth's Deep Water Cycle (pp. 251-261)
Talavera-Soza, S., Cobden, L., Faul, U., & Deuss, A. (2023). Global 3D model of mantle attenuation using seismic normal modes. Research Square. https://doi.org/10.21203/rs.3.rs-1580818/v1